Part S1 Experimental section

Chemicals: All the chemical reagents and solvents were obtained at analytical grade and utilized without further purification. These reagents were: anhydrous acetonitrile (CH_3CN), ethanol (C_2H_5OH), phenol (C_6H_5OH), carbazole ($C_{12}H_9N$), p-dimethylaminobenzaldehyde ($C_9H_{11}NO$), $C_5FeN_6Na_2O$ (sodium nitroferricyanide), lithium perchlorate ($LiClO_4$), acetone (C_3H_6O), copper (II) sulfate pentahydrate ($CuSO_4$-$5H_2O$), lactic acid 30% ($C_3H_6O_3$), hydrochloric acid fuming (37%), sodium hydroxide (NaOH), hydrazine (N_2H_4), ammonium chloride (NH_4Cl), sodium sulfate (Na_2SO_4), sodium nitrite ($NaNO_2$) and sodium nitrate ($NaNO_3$). All of these were purchased from Merck. Nitrogen gas (N_2, 99.999%) and argon gas (Ar, 99.999%) were purchased from INDURA S.A. In addition, Ultrapure water (Millipore Milli-Q grade, 18.20 MΩ) was used for synthetic and electrocatalytic purposes.

Synthesis of PCz/Cu_2O: The proposed electrode was prepared by electrochemical deposition of polycarbazole (PCz) on the surface of an FTO electrode, followed by the deposition, by chronopotentiometry, of Cu_2O (Figure S1). The proposed methodology is a facile and low-cost synthesis. Three cycles of cyclic voltammetry between potentials from 0 to 2 V are performed on the FTO film, using an acetonitrile solution containing 0.1 M $LiClO_4$ and 0.01 M carbazole. For this purpose, a one-compartment cell is used, in which a FTO foil participates as working electrode, a platinum wire as counter electrode and a saturated Ag/AgCl electrode as reference electrode. After the deposition process is completed, the resulting electrode is rinsed with acetone and subsequently dried using an Argon flow.

Subsequently, the PCz electrode was used as a cathodic working electrode in a three-compartment electrochemical cell. A platinum (Pt) wire was used as counter electrode and saturated Ag/AgCl as reference electrode. The electrochemical cell was filled with an aqueous solution of 0.5 M $CuSO_4$-$5H_2O$ and 4 M lactic acid at pH 12.5 (this pH was adjusted with NaOH). The cell with the solution was purged with argon gas for 20 min. A current density of -1 mA cm^{-2} was then applied for 5 min using a potentiostat/galvanostat (Vertex, IVIUM technologies). The solution was continuously stirred during the experiment. The generated electrode PCz/Cu_2O is washed with deionized water several times, then dried and stored in the dark.

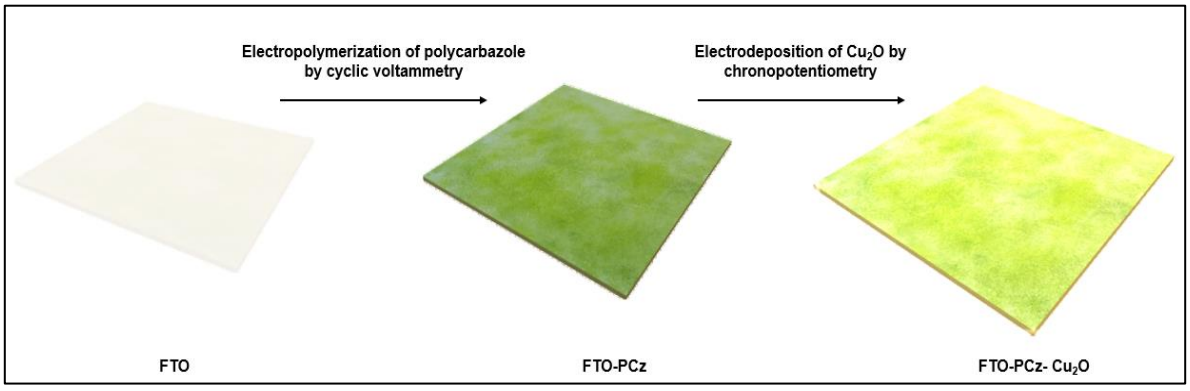

Figure S1: Schematic of the preparation process of Cu_2O nanoparticles on a polycarbazole coated FTO glass substrate.

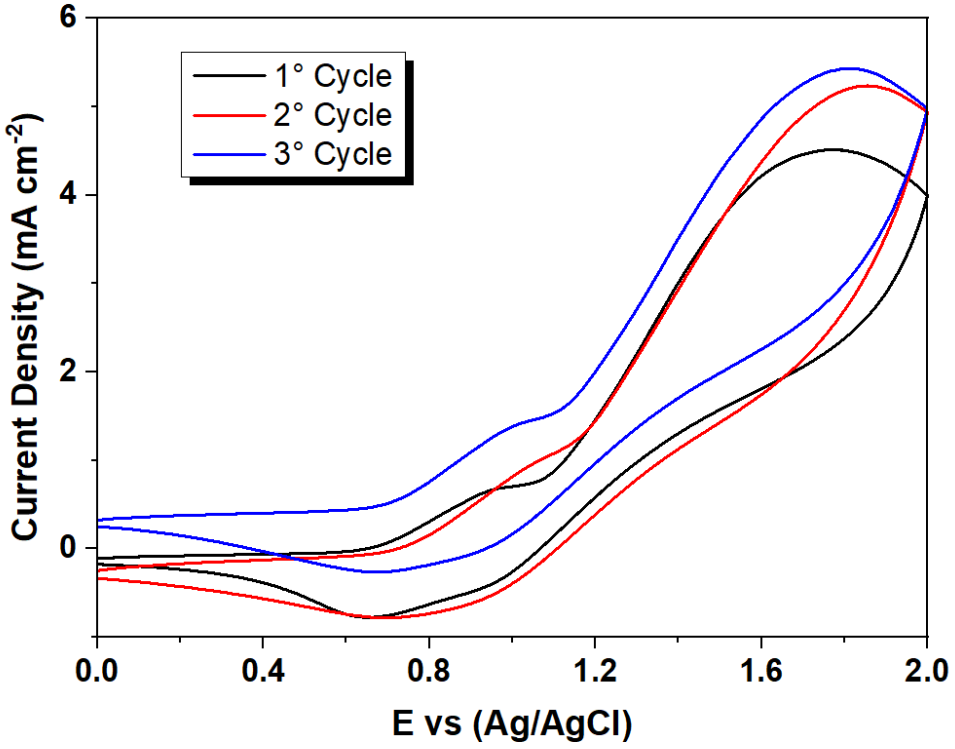

Figure S2: Cyclic voltammetry of carbazole deposition on FTO glass. Performed in 0.01M Carbazole solution and 0.1M lithium perchlorate supporting electrolyte, with 3 deposition cycles at a scan rate of 50mV/s.

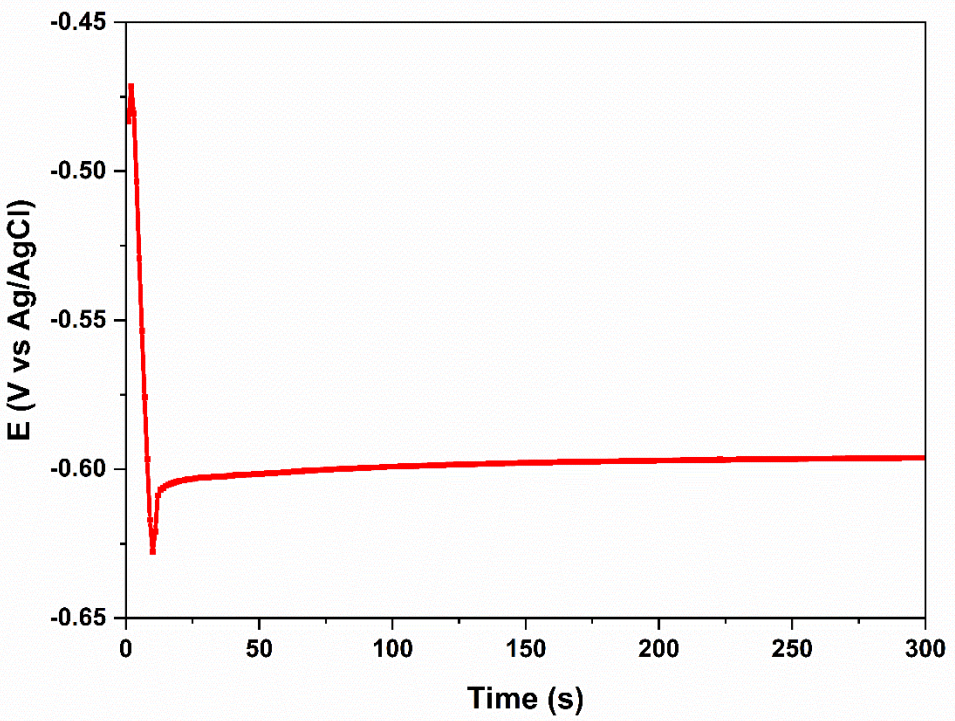

Figure S3: Chronopotentiometry of Cu_2O on FTO-PCz electrode

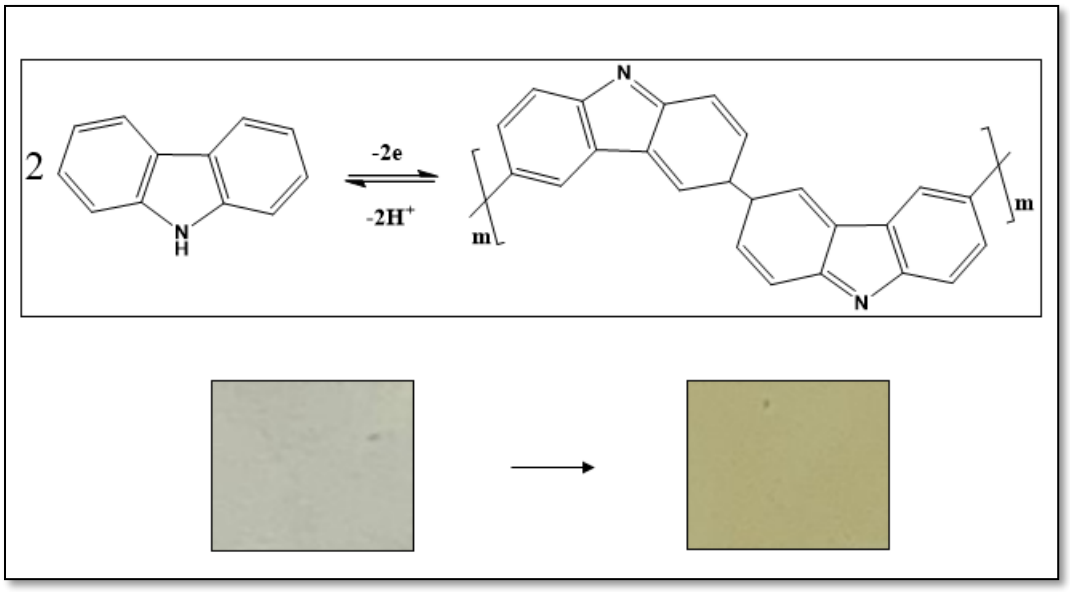

Figure S4: Schematic representation of Carbazole polymerization and electrode coloration change (FTO) in the presence of polymer deposition.

Characterization:

- Field emission scanning electron microscope (FESEM) and energy dispersive X-ray spectroscopic (EDS) was performed using a Quanta FEG25 model microscope equipped with a Silicon Drift Detector (SDD), Octane Pro model of 10 mm2 detection area. The instrument has a resolution of 130eV and resolution stability over 90% up to 200 kcps. The electrodes were pretreated by gently heating at 50°C overnight using a stationary vacuum oven. The samples were then fixed in the sample holder and exposed to the environment for the short period of time (~20 s) necessary to load them into the FESEM instrument.

- X-ray photoelectron spectroscopic (XPS) was performed with a FlexPS-CIENUC instrument, brand SPECS (Berlin, Germany), which is equipped with an XR 50 (Al/Ag) dual-anode X-ray source, a FOCUS 500 monochromator and a Phoibos 150 hemispherical analyzer. The analysis chamber was maintained at a pressure of 2 x 10^{-10} mbar. Probe sweeps were recorded with a step energy of 200 eV and a step size of 1 eV, while high-resolution data were obtained with a step energy of 50 eV and a step size of 0.1 eV. The samples were kept in ultra-high vacuum overnight before XPS measurements were performed. There was no electrical contact between the sample and the instrument ground, and the samples were charge neutralized prior to analysis. The collected spectral data were energetically corrected by fitting the aliphatic C-C peak in the C 1s spectra at 284.52 eV.

- Fourier-transform infrared – attenuated total reflectance (FTIR-ATR) using a Nicolet iS10 FTIR ATR spectrophotometer equipped with a gold mirror as ATR crystal. Spectra (average of 30 scans) were collected at ambient conditions between 4000 and 400 cm^{-1} with a resolution of 5 cm^{-1}.

- Atomic force microscope (AFM) and Raman were collected using a WiTec Alpha 300 RA Raman-AFM using 532 and 750 nm lasers.

- X-ray diffraction (XRD) Structural characterization of the samples has been examined by X-ray diffraction measurements, carried out with standard theta–2 theta scans on a Philips PW180 diffractometer (30 kV, 40 mA, CuKα radiation with λ = 1.5406 Å).
- Transmission Electron Microscope (TEM) TEM images were obtained using Hitachi HT7700 equipment. The TEM microscope allows to obtain images at a nanometer scale with a resolution of 0.2 nm.

Electrochemical measurements:

All electrochemical measurements were performed with a potentiostat/galvanostat (Vertex IVIUM Technologies) using an H-type split cell. A Nafion® 117 ion exchange membrane was used to separate the cathode and anode. Before use, the Nafion 117 membrane was treated according to the standard treatment method and heated continuously for 1 h in an aqueous solution of H_2O_2, 0.50 M H_2SO_4 and ultrapure water at 80°C, respectively. The treated membrane was then stored in deionized water at room temperature for later use.

The electrodes used were: FTO/PCz/Cu_2O as working electrode (with a working area of 1.00 × 1.00 cm^2), a graphite electrode as counter electrode and Ag/AgCl sat. as reference electrode. All potentiostatic NRR measurements were carried out in 30 mL of 0.1 M Na_2SO_4 electrolyte at room temperature (25°C), to which 0.01 M of the ionic species to be reduced in the respective electrolysis ($NaNO_3$ or $NaNO_2$) was added separately and purged using argon gas. In the case of reduction with N_2, the Na_2SO_4 solution is bubbled at constant flow with N_2 to saturate it prior to electrolysis; during the measurement, the N_2 flow remains constant but in a shallow manner inside the cell (bubbling is interrupted). Open circuit potential curves (OCP) were collected after the potential (Eoc) was stabilized to ±0.1 mV or after 2 h. Then, electrochemical impedance spectroscopy (EIS) was measured at the OCP values stabilized over a frequency range from 20 kHz to 3 mHz with 8 points per decade, using 10 mV peak-to-peak sinusoidal voltage centered at E=Eoc.

Material cleaning

To remove possible contaminants on the glassware, careful washing of the glassware with a NaOH solution of pH ≥ 10 is recommended. For cleaning the nafion membrane, it is recommended to wash it with successive H_2SO_4 and H_2O_2 washes for each electrolysis, table S1 summarizes the steps of the nafion membrane prior to electrolysis. Possible contamination of the electrolyte is controlled by measuring a small amount of electrolyte by colorimetry before electrolysis. Finally, to confirm the glass material's cleanliness and evaluate the possible decomposition of the compounds used as electro-catalysts, electrolysis in the Ar atmosphere must be carried out under the same conditions chosen for the electrolysis with N_2. Subsequently, the NH_3 generated in this electrolysis is quantified [1]. The detection of NH_3 in the electrolysis with Ar would confirm the presence of nitrogen contaminants and/or the decomposition of the working electrode.

Table S1: Steps for nafion membrane washing recommended [1], [2].

	Ultrasonic bath
Nafion membrane washing	20 minutes in H_2O_2 5%
	20 minutes in H_2O nanopure
	20 minutes in H_2SO_4 0,5 M
	20 minutes in H_2O nanopure
	12 hours in H_2O nanopure at 80°C

	Sonication before electrolysis in H_2SO_4 0.05 M

DEMS Metodology

The DEMS (Differential Electrochemical Mass Spectrometry) methodology is an analytical method that combines mass spectrometry and electrochemical experimentation in a cell. It is used in continuous faradaic reactions to identify products or intermediates and to characterize adsorbates on electrode surfaces by adsorption. DEMS allows in situ determination of the resolved mass of reaction intermediates, gaseous or volatile electrochemical reagents, and products in real time. A typical DEMS system comprises an electrochemical half-cell, a membrane interface, and a vacuum system including a quadrupole mass spectrometer [3]. In the present case, it is used to demonstrate the null presence of NO_x pollutants in the nitrogen used in the catalysis, to avoid possible false positives, around the reduction of other compounds than the N_2 supplied.

Mass spectra were acquired in a Hiden HPR40 dissolved species mass spectrometer, using a DEMS type cell (Figure S5), to which a constant flow of electrolyte ($NaSO_4$ 0.1M) was passed, together with a constant flow of nitrogen. Parallel to this, the whole experiment was performed at open circuit potential with the help of potentiostat/galvanostat (Vertex, IVIUM technologies).

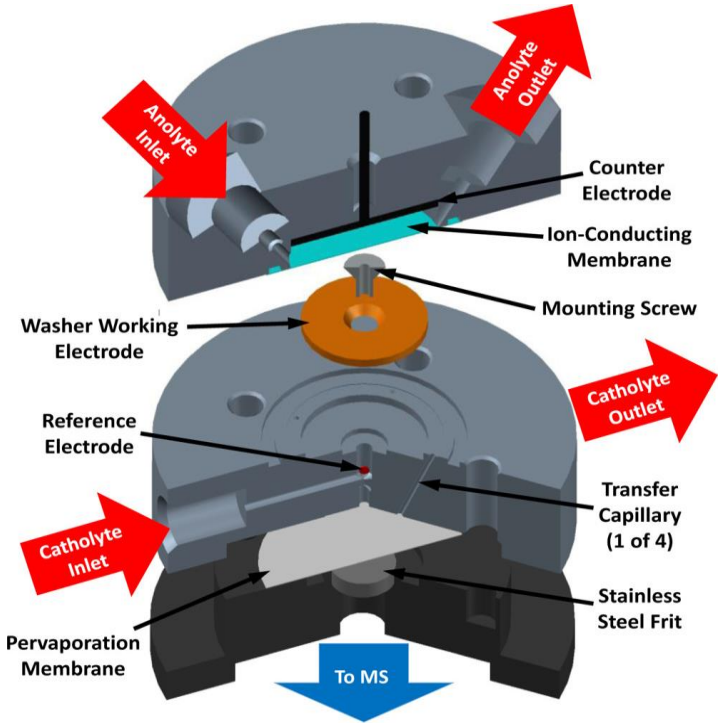

Figure S5: Schematic of DEMS cell [4]

An electron energy of 70 eV was used for ionization of all species, with an emission current of 500 µA. The ions detected were (Figure S6): hydrogen (m/z = 1), (m/z = 2); nitrogen (m/z = 14), (m/z = 28) water (m/z = 17), (m/z = 18) and oxygen (m/z = 32). They were also accelerated with a voltage of 3 V to maximize the detector response. All mass-selected product cations were detected using a secondary electron multiplier with a

detector voltage of 875 V. These mass spectrometer settings were determined to be optimal for maximizing the signal-to-noise ratio of the liquid-phase products. With these settings, a data point was recorded every 1s. Data were obtained using a cell at open circuit potential for 60 min with continuous nitrogen flow.

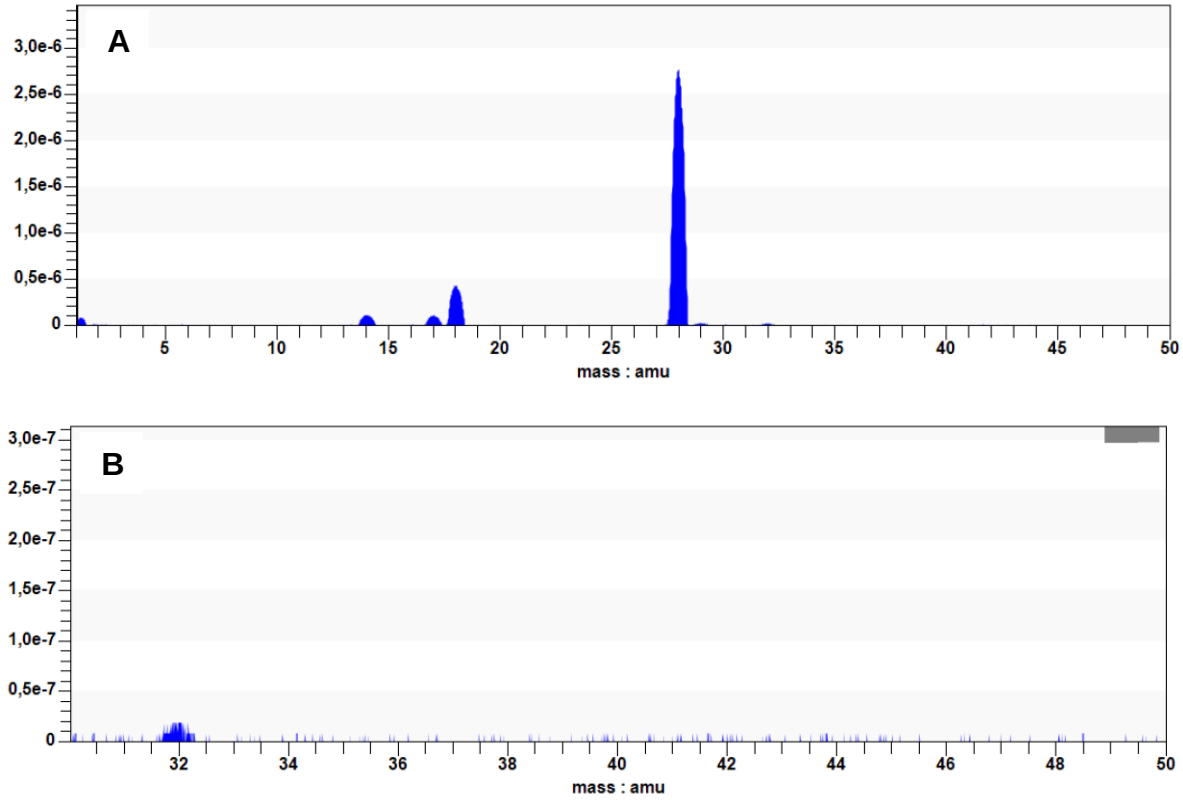

Figure S6: DEMS spectrum. (A) Mass spectrum m/z = 0-50; (B) Extended spectrum between m/z = 28-50.

It should be noted that this type of equipment has a sensitivity of 1 ppb, which translates into a minimum concentration of 0.033 µM. Based on this, considering the reduction of N_2 at -0.8 V potential, in which an average concentration of 7.1 µM of ammonia was obtained. It can be deduced that the maximum percentage of ammonia that can be obtained through NOx present as a contaminant of the N2 pond is 0.47%. This indicates that 99.53% of the ammonia generated comes directly from the reduction of N_2.

From this, and by not observing ionic responses for NOx-derived compounds such as NO (m/z = 30), N_2O (m/z = 44), and NO_2 (m/z = 46). We can indicate that the NO_x that could exist in the N_2 cylinder is negligible, and the ammonia contribution generated through it is practically null. This is because the minimum contribution of ammonia generated through N_2 would be 99.53%.

Determination of ammonia (NH_3):

The concentration of the ammonia produced was determined by the indophenol blue method [5]. In all cases, 10 mL of the electrolyte was removed after the NRR potentiostatic test, and 0.4 mL of the solution containing 5 g of phenol in 50 ml of ethanol and 0.4 mL of 0.5 wt.% $C_5FeN_6Na_2O$ (sodium nitroferricyanide) were added successively. Then, 1 ml of oxidizing solution containing 10 g sodium citrate, 0.5 g sodium hydroxide, and 10 ml sodium hypochlorite in 50 ml Millipore water was also added to the above solution. The UV-Vis absorption spectrum was measured after storing the mixture in the dark at room temperature for 2 h. The concentration of indophenol blue was measured as a function of absorbance at a wavelength of 633 nm. Standard solutions

of NH_4Cl at a series of concentrations in 0,1 M Na_2SO_4 were prepared to construct calibration curves and quantify the ammonia produced.

In 0,1 M Na_2SO_4, the curve fit was y = 0.22x - 0.038 (R^2 = 0.995) after three independent calibrations, and the absorbance value showed a good linear relationship with NH_4^+ concentration (Figure S7). The NH_3 yield reported in this work was the total NH_3 collected from the cathodic and anodic chambers.

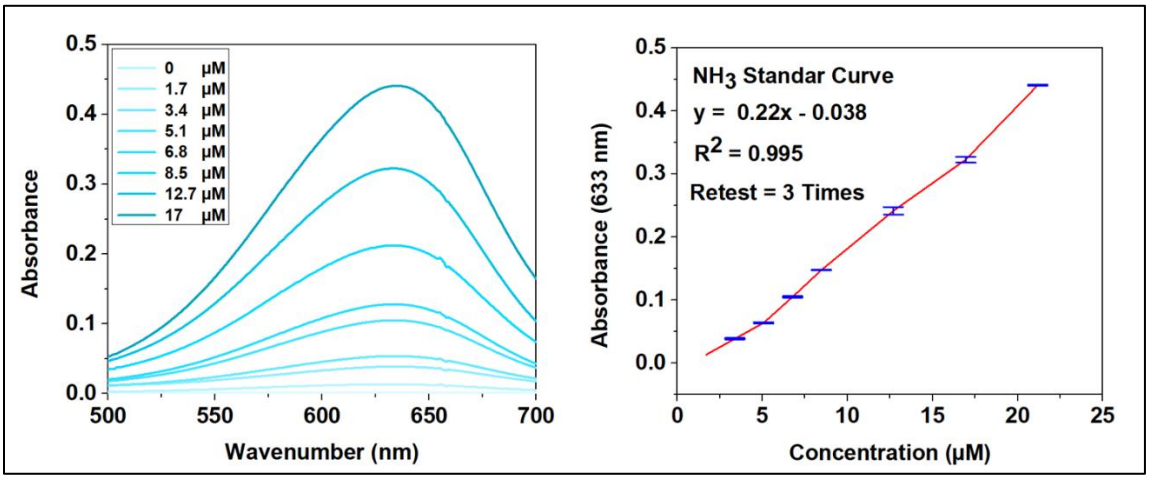

Figure S7: Determination of ammonia produced in 0.1 M Na_2SO_4 at 633 nm. UV-Vis absorption spectra (left) and corresponding calibration curves for the colorimetric assay of NH_3 by the indophenol blue method (right).

Determination of hydrazine (N_2H_4):

The concentration of the hydrazine produced was determined by the method of Watt and Chrisp [5]. In both cases, a mixture of ethanol (300 ml), HCl (concentrate, 30 ml) and p-dimethylaminobenzaldehyde (5.99 g) was used as color reagent. For this purpose, 10 ml of the residual electrolyte was removed after the potentiostatic NRR test and 10 ml of the previously prepared color reagent was added successively. The resulting solution was stirred for 10 min at room temperature and its absorbance was measured at a wavelength of 457 nm. Hydrazine standard solutions were previously prepared at a series of concentrations in 0.1 M Na_2SO_4 to construct calibration curves and quantify the hydrazine produced. The calibration curve obtained from N_2H_4 (y = 0,066x + 0,015, R^2 = 0.999) was used for the quantitative assay (Figure S8).

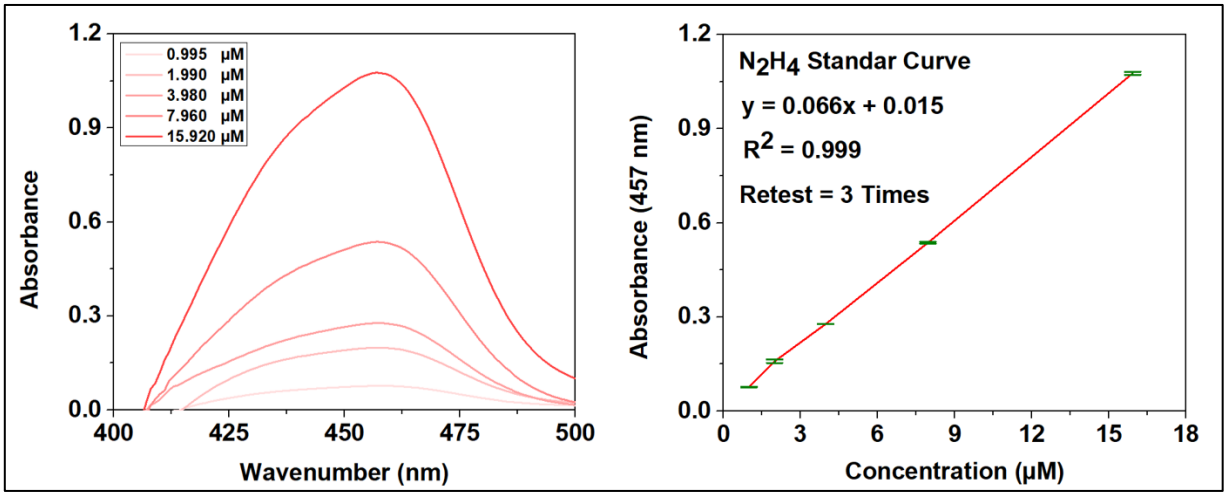

Figure S8: Determination of hydrazine produced in 0.1 M Na_2SO_4 at 457 nm. UV-Vis absorption spectra (left) and corresponding calibration curves for the colorimetric assay of N_2H_4 by the Watt y Chrisp method (right).

Determination of NH_3 and N_2H_4 yields:

- R_{NH3} was calculated by the following equation:

$$R_{NH_3}(\mu g\ h^{-1}cm^{-2}) = \frac{C_{NH_3}(\mu g\ mL^{-1})\ x\ V\ (mL)}{t\ (h) x\ A_{cat}(cm^2)}$$

Where $\mathbf{C_{NH3}}$ is the NH_3 concentration, **V** is the volume of the electrolyte solution, **t** is the NRR reaction time and $\mathbf{A_{cat}}$ is the catalyst area.

- R_{N2H4} was calculated by the following equation:

$$R_{N_2H_4}(\mu g\ h^{-1}cm^{-2}) = \frac{C_{N_2H_4}(\mu g\ mL^{-1})\ x\ V\ (mL)}{t\ (h) x\ A_{cat}(cm^2)}$$

Where $\boldsymbol{C_{N_2H_4}}$ is the N_2H_4 concentration, **V** is the volume of the electrolyte solution, **t** is the NRR reaction time and $\mathbf{A_{cat}}$ is the catalyst area.

Calculations of faradaic efficiency (FE):

- The EF for NH_3 was calculated using the following equation:

$$FE(\%) = \frac{n_e\ x\ n_{NH_3}(mol)\ x\ F\ (Cmol^{-1})}{Q\ (C)}$$

Where $\mathbf{n_e}$ is the number of electrons involved in the reduction, this depends on the source species. Specifically, for NO_3^- and NO_2^- ions it is 8 and 6 respectively. Similarly, for N_2 gas the number of electrons involved is 3. On the other hand, $\mathbf{n_{NH3}}$ corresponds to the moles of ammonia generated, **F** is the Faraday constant (96485 C mol^{-1}), and **Q** is the total charge transferred during the NRR.

- The EF for N_2H_4 was calculated using the following equation:

$$\boldsymbol{FE}(\%) = \frac{\boldsymbol{n_e\ x\ n_{N_2H_4}(mol)\ x\ F\ (Cmol^{-1})}}{\boldsymbol{Q\ (C)}}$$

Where $\mathbf{n_e}$ is the number of electrons involved in the reduction, this depends on the source species. Specifically, for NO_3^- and NO_2^- ions it is 7 and 5 respectively. Similarly, for N_2 gas the number of electrons involved is 2. On the other hand, $\mathbf{n_{NH3}}$ corresponds to the moles of ammonia generated, **F** is the Faraday constant (96485 C mol^{-1}), and **Q** is the total charge transferred during the NRR

Part S2 Stability results

- Stability results

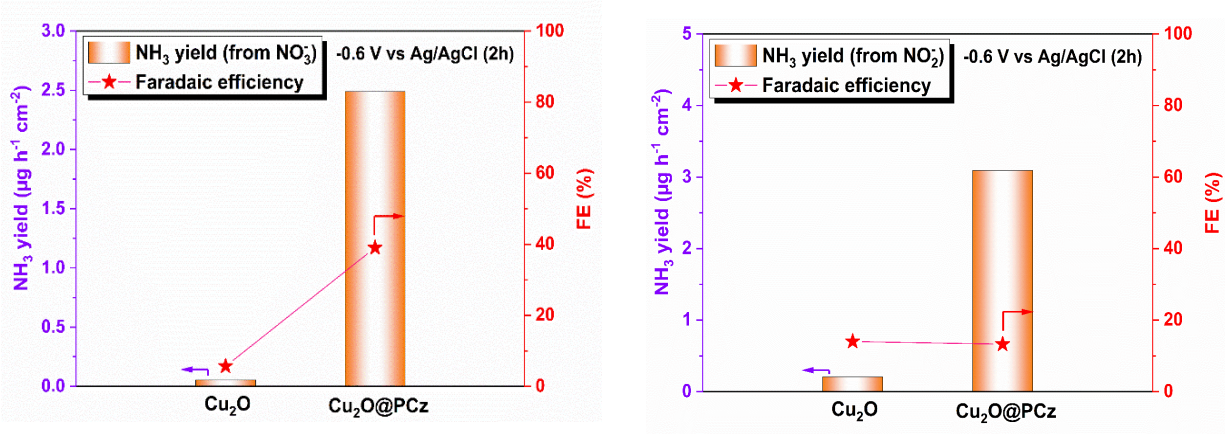

Figure S9: Faradaic efficiency and generation rate to different potentials for ammonia, for electroreduction of (A) NO_3^-, (B) NO_2^-.

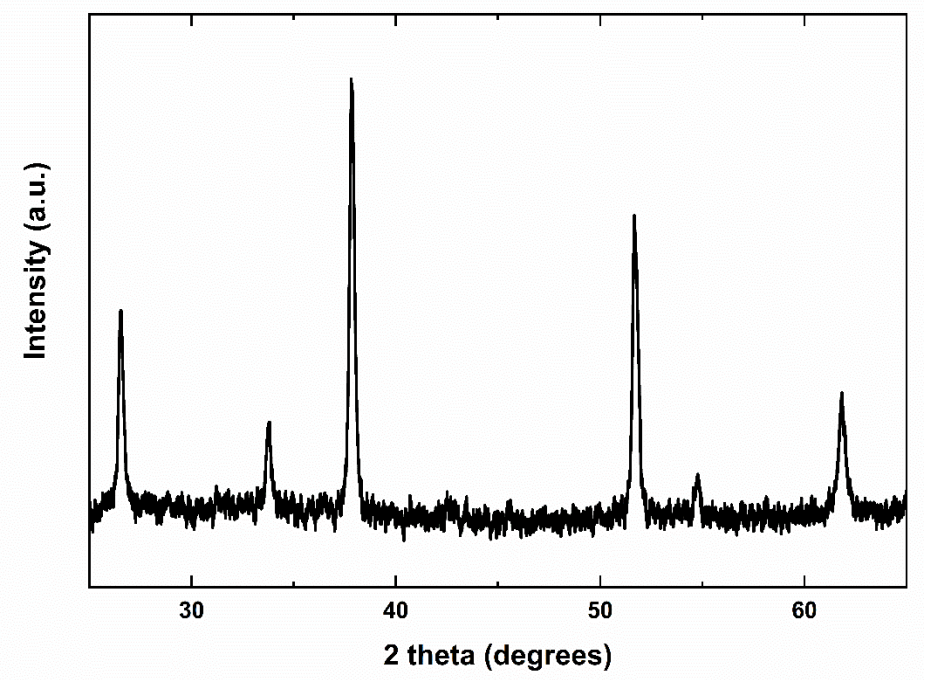

Figure S10: X-ray diffraction pattern of the Cu_2O@PCz electrode

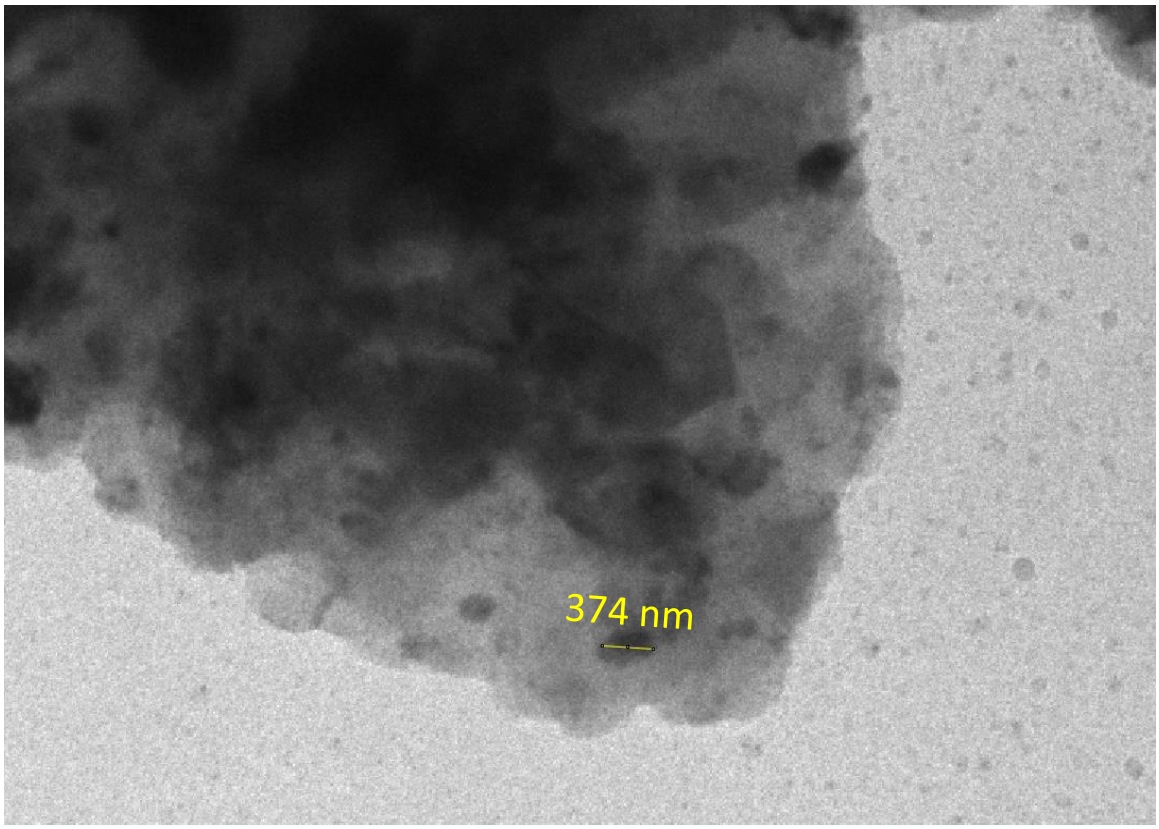

Figure S11: TEM image of Cu2O@PCz electrode after electrolysis.

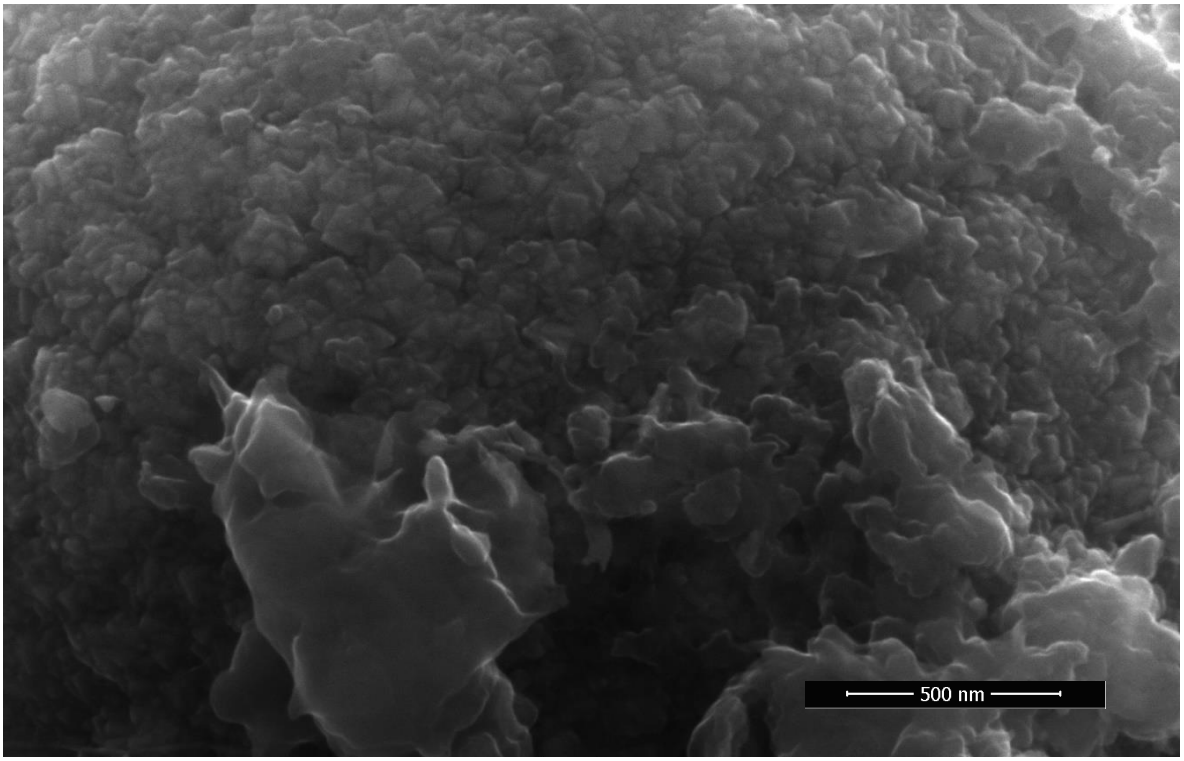

Figure S12: Magnification FE-SEM image of Cu2O@PCz electrode after electrolysis (Fig. 10).

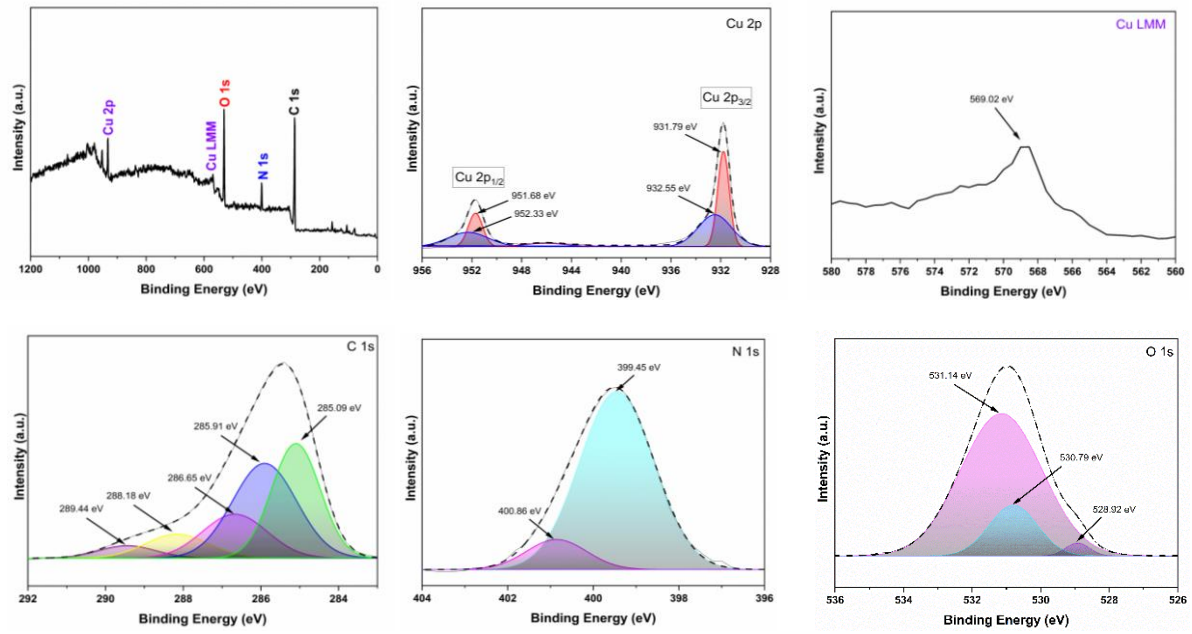

Figure S13: Spectroscopical analysis XPS of Cu_2O@PCz electrode after catalisis. (A) Survey spectra; (B) Cu 2p; (C) Cu 2p AES (Auger electron spectroscopy).; (D) C 1s; (E) N 1s; and (F) O 1s.

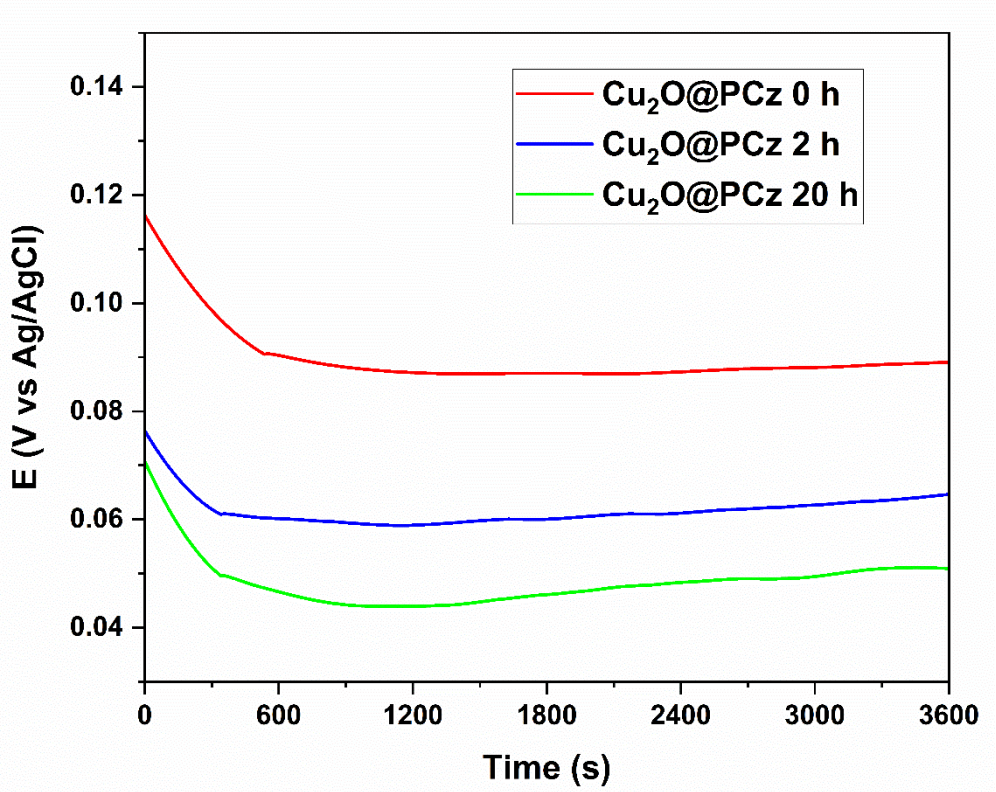

Figure S14: Cu2O@FTO OCP at different NRR times.

Part S3 Electrocatalytic results

- Comparative tables

Table S2: Faradaic efficiencies and generation rates obtained for the reduction of different nitrogenous compounds.

Catalyst	Species to be reduced	Species generated	Selectivity (%)	Performance (μg $h^{-1} cm^{-2}$)	Potential (V)
FTO-PCz-Cu_2O	NO_3^-	NH_3	39.042	2.495	-0.6
	NO_3^-	N_2H_4	0.049	0.007	–0.6
	NO_2^-	NH_3	19.039	3.631	-0.4
	NO_2^-	N_2H_4	77.721	37.026	-0.8
	N_2	NH_3	38.825	1.811	-0.8
	N_2	N_2H_4	7.385	0.768	-0.4

Table S3: Comparison of different catalysts for NRR

Catalyst	Electrolyte	Selectivity (% NH_3)	Performance (μg $h^{-1} cm^{-2}$ / μg $h^{-1} mg^{-1}$)	Potential (V)	Ref.
FTO-PCz-Cu_2O	0.1 M Na_2SO_4	38.82	1.81 / -	-0.8[b]	This work
PdCu/rGO	0.1 M KOH	~4.5	- / 2.80	–0.2[a]	[6]
Au/CeOx-RGO	0.1 M HCl	10.1	- / 8.3	-0.2[a]	[7]
rGO/Fe@Fe_3O_4/ CP	0.2 M $NaHCO_3$	6.25	7.956 / -	-0.3[a]	[8]
ZnO/RGO	0.1 M Na_2SO_4	6.4	- / 17.7	-0.65[a]	[9]
TiO2/RGO	0.1 M Na_2SO_4	3.3	- / 15.13	-0.9[a]	[10]
CoS_2/NS-G	0.05 M H_2SO_4	25.9	- / 25	–0.05[a]	[11]
PdCu@UiO-S@PDMS	0.1 M HCl	13.16	-/20.24	–0.25[a]	[12]
V_2O_3/VN	0.1 M KOH	18.9	219.6/-	-0.3[a]	[13]
$PdFe_3$	0.1 M KOH	22.8	-/29.07	-0.2[a]	[14]
A-Mo-MoS_2	0.5 M H_2SO_4	27.3	-/48.8	-0.2[a]	[15]
CuAg alloy	0.1 Na_2SO_4	12.72	38.35/-	-0.6[a]	[16]
1T/2H MoSSe	0.1 M HCl	12.66	-/32.32	-0.45[a]	[17]

a: The numbers were potentials relative to the reversible hydrogen electrode (RHE).

b: The numbers were potentials relative to the saturated of Ag/AgCl

Table S4: Comparison of different catalysts in nitrate electroreduction

Catalyst	Electrolyte	Selectivity (% NH_3)	Performance (μg h^{-1} cm^{-2} / μg h^{-1} mg^{-1})	Potential (V)	Ref.
FTO-PCz-Cu_2O	0.1 M Na_2SO_4 + 0.01 M KNO3	39.04	2.495 / -	-0.6[c]	This work
Cu@C	1 mM NO_3^- + 1 M KOH	72.0	469.5 / -	−0.9[a]	[18]
CuCoSP	1 mM NO_3^- + 0.1 M KOH	91.2	267.0 / -	-0.155[a]	[19]
PdCoO/NF	0.5 M K_2SO_4 + 200 mg L^{-1} NO_3^-	95.3	3474.8 / -	−1.3[b]	[20]
Ag/Cu2O	0.5 M Na_2SO_4 + 100 ppm NO_3^-	96.45	3825 / -	-0.8[a]	[21]
CuNi NPs/CF	1 M NaOH + 44.3 g L^{-1} NO_3	97.03	94.57 / -	−0.48[a]	[22]
Fe-CoS_2	0.5 M Na_2SO_4 + 0.1 M $NaNO_3$	97.5	10800/ -	-0.6[a]	[23]
Fe_2TiO_5	phosphate buffer + 0.1 M $NaNO_3$	87.6	-/ 12431.9	−0.9[a]	[24]
Au/Cu SAA	0.5 M Na_2SO_4 + 100 ppm NO_3^-	99.69	3284.79 / -	-0.8[a]	[25]
Cu/MnO_x	0.1 M Na_2SO_4 + 10 mM KNO_3	98.2	5530/-	-0.6[a]	[26]
Co_3O_4/Co-h	0.1 M Na_2SO_4 + 1mg mL^{-1} NO_3^-	88.7	4430/-	−0.9[a]	[27]
$CoCuO_x$@CuO_x/ CF	0.1 M KOH + 1 mM NO_3^-	99.83	519.1/-	−0.2[a]	[28]

a: The numbers were potentials relative to the reversible hydrogen electrode (RHE).

b: The numbers were potentials relative to the saturated calomel electrode (SCE).

c: The numbers were potentials relative to the saturated of Ag/AgCl

References

[1] J. Choi *et al.*, "Identification and elimination of false positives in electrochemical nitrogen reduction studies," *Nat Commun*, vol. 11, no. 1, Dec. 2020, doi: 10.1038/s41467-020-19130-z.

[2] F. Hanifpour, A. Sveinbjörnsson, C. P. Canales, E. Skúlason, and H. D. Flosadóttir, "Preparation of Nafion Membranes for Reproducible Ammonia Quantification in Nitrogen Reduction Reaction Experiments," *Angewandte Chemie - International Edition*, vol. 59, no. 51, pp. 22938–22942, Dec. 2020, doi: 10.1002/anie.202007998.

[3] H. Baltruschat, "Differential electrochemical mass spectrometry," *J Am Soc Mass Spectrom*, vol. 15, no. 12, pp. 1693–1706, 2004, doi: 10.1016/j.jasms.2004.09.011.

[4] E. L. Clark, M. R. Singh, Y. Kwon, and A. T. Bell, "Differential Electrochemical Mass Spectrometer Cell Design for Online Quantification of Products Produced during Electrochemical Reduction of CO2," *Anal Chem*, vol. 87, no. 15, pp. 8013–8020, Aug. 2015, doi: 10.1021/acs.analchem.5b02080.

[5] M. Wang *et al.*, "Over 56.55% Faradaic efficiency of ambient ammonia synthesis enabled by positively shifting the reaction potential," *Nat Commun*, vol. 10, no. 1, Dec. 2019, doi: 10.1038/s41467-018-08120-x.

[6] M. M. Shi, D. Bao, S. J. Li, B. R. Wulan, J. M. Yan, and Q. Jiang, "Anchoring PdCu Amorphous Nanocluster on Graphene for Electrochemical Reduction of N2 to NH3 under Ambient Conditions in Aqueous Solution," *Adv Energy Mater*, vol. 8, no. 21, Jul. 2018, doi: 10.1002/aenm.201800124.

[7] S. J. Li, D. Bao, M. M. Shi, B. R. Wulan, J. M. Yan, and Q. Jiang, "Amorphizing of Au Nanoparticles by CeOx–RGO Hybrid Support towards Highly Efficient Electrocatalyst for N2 Reduction under Ambient Conditions," *Advanced Materials*, vol. 29, no. 33, Sep. 2017, doi: 10.1002/adma.201700001.

[8] C. Li, Y. Fu, Z. Wu, J. Xia, and X. Wang, "Sandwich-like reduced graphene oxide/yolk-shell-structured Fe@Fe3O4/carbonized paper as an efficient freestanding electrode for electrochemical synthesis of ammonia directly from H2O and nitrogen," *Nanoscale*, vol. 11, no. 27, pp. 12997–13006, Jul. 2019, doi: 10.1039/c9nr02782c.

[9] Y. ping Liu, Y. biao Li, D. jian Huang, H. Zhang, and K. Chu, "ZnO Quantum Dots Coupled with Graphene toward Electrocatalytic N2 Reduction: Experimental and DFT Investigations," *Chemistry - A European Journal*, vol. 25, no. 51, pp. 11933–11939, Sep. 2019, doi: 10.1002/chem.201902156.

[10] X. Zhang *et al.*, "TiO2 nanoparticles-reduced graphene oxide hybrid: An efficient and durable electrocatalyst toward artificial N2 fixation to NH3 under ambient conditions," *J Mater Chem A Mater*, vol. 6, no. 36, pp. 17303–17306, 2018, doi: 10.1039/c8ta05627g.

[11] P. Chen *et al.*, “Interfacial engineering of cobalt sulfide/graphene hybrids for highly efficient ammonia electrosynthesis,” *Proc Natl Acad Sci U S A*, vol. 116, no. 14, pp. 6635–6640, Apr. 2019, doi: 10.1073/pnas.1817881116.

[12] L. Wen, K. Sun, X. Liu, W. Yang, L. Li, and H.-L. Jiang, “Electronic State and Microenvironment Modulation of Metal Nanoparticles Stabilized by MOFs for Boosting Electrocatalytic Nitrogen Reduction,” *Advanced Materials*, vol. 35, no. 15, p. 2210669, Apr. 2023, doi: https://doi.org/10.1002/adma.202210669.

[13] T.-Y. An *et al.*, “V2O3/VN electrocatalysts with coherent heterogeneous interfaces for selecting low-energy nitrogen reduction pathways,” *SusMat*, vol. n/a, no. n/a, p. e226, Jul. 2024, doi: https://doi.org/10.1002/sus2.226.

[14] J. Mu *et al.*, “Bimetallic PdFe3 Nano-Alloy with Tunable Electron Configuration for Boosting Electrochemical Nitrogen Fixation,” *Adv Energy Mater*, vol. 14, no. 8, p. 2303558, Feb. 2024, doi: https://doi.org/10.1002/aenm.202303558.

[15] G. Zhan *et al.*, “Single-layer MoS2 with adjacent Mo sites for efficient electrocatalytic nitrogen fixation via spin-delocalized electrons effect,” *Appl Catal B*, vol. 323, p. 122186, 2023, doi: https://doi.org/10.1016/j.apcatb.2022.122186.

[16] Z. Wei, Z. Gu, Y. Zhang, K. Luo, and S. Zhao, “Phase-separated CuAg alloy interfacial stress induced Cu defects for efficient N2 activation and electrocatalytic reduction,” *Appl Catal B*, vol. 320, p. 121915, 2023, doi: https://doi.org/10.1016/j.apcatb.2022.121915.

[17] M. Sun *et al.*, “Electrochemical ammonia synthesis via nitrogen reduction reaction on 1T/2H mixed-phase MoSSe catalyst: Theoretical and experimental studies,” *Materials Today Physics*, vol. 30, p. 100945, 2023, doi: https://doi.org/10.1016/j.mtphys.2022.100945.

[18] Z. Song, Y. Liu, Y. Zhong, Q. Guo, J. Zeng, and Z. Geng, “Efficient Electroreduction of Nitrate into Ammonia at Ultralow Concentrations Via an Enrichment Effect,” *Advanced Materials*, vol. 34, no. 36, Sep. 2022, doi: 10.1002/adma.202204306.

[19] W. He *et al.*, “Splicing the active phases of copper/cobalt-based catalysts achieves high-rate tandem electroreduction of nitrate to ammonia,” *Nat Commun*, vol. 13, no. 1, Dec. 2022, doi: 10.1038/s41467-022-28728-4.

[20] M. Liu *et al.*, “Electroreduction of Nitrate to Ammonia on Palladium-Cobalt-Oxygen Nanowire Arrays,” *ACS Appl Mater Interfaces*, vol. 14, no. 11, pp. 13169–13176, Mar. 2022, doi: 10.1021/acsami.1c19412.

[21] H. Yin *et al.*, “New insight on electroreduction of nitrate to ammonia driven by oxygen vacancies-induced strong interface interactions,” *J Catal*, vol. 406, pp. 39–47, Feb. 2022, doi: 10.1016/j.jcat.2021.12.031.

[22] W. Yu *et al.*, “Laser-controlled tandem catalytic sites of CuNi alloys with ampere-level electrocatalytic nitrate-to-ammonia reduction activities for Zn–nitrate batteries,” *Energy Environ Sci*, vol. 16, no. 7, pp. 2991–3001, 2023, doi: 10.1039/D3EE01301D.

[23] N. Zhang, G. Wang, G. Zhang, K. Chen, and K. Chu, “Electrochemical nitrate-to-ammonia reduction over atomic Fe-dopants incorporated in CoS2,” *Chemical Engineering Journal*, vol. 474, p. 145861, 2023, doi: https://doi.org/10.1016/j.cej.2023.145861.

[24] H. Du *et al.*, “Durable Electrocatalytic Reduction of Nitrate to Ammonia over Defective Pseudobrookite Fe2TiO5 Nanofibers with Abundant Oxygen Vacancies,” *Angewandte Chemie International Edition*, vol. 62, no. 5, p. e202215782, Jan. 2023, doi: https://doi.org/10.1002/anie.202215782.

[25] H. Yin, Y. Peng, and J. Li, “Electrocatalytic Reduction of Nitrate to Ammonia via a Au/Cu Single Atom Alloy Catalyst,” *Environ Sci Technol*, vol. 57, no. 8, pp. 3134–3144, Feb. 2023, doi: 10.1021/acs.est.2c07968.

[26] Y. Cui *et al.*, “Interfacially Engineered Nanoporous Cu/MnO Hybrids for Highly Efficient Electrochemical Ammonia Synthesis via Nitrate Reduction,” *Small*, vol. 19, no. 17, p. 2207661, Apr. 2023, doi: https://doi.org/10.1002/smll.202207661.

[27] F. Zhao, G. Hai, X. Li, Z. Jiang, and H. Wang, “Enhanced electrocatalytic nitrate reduction to ammonia on cobalt oxide nanosheets via multiscale defect modulation,” *Chemical Engineering Journal*, vol. 461, p. 141960, 2023, doi: https://doi.org/10.1016/j.cej.2023.141960.

[28] C. Xiao *et al.*, “Efficient electrocatalytic reduction of nitrate to ammonia at low concentration by copper-cobalt oxide nanowires with shell–core structure,” *Nano Res*, vol. 17, no. 6, pp. 5087–5094, 2024, doi: 10.1007/s12274-024-6530-8.